

On the Outskirts of Dark Matter Haloes

Alice Y. Chen*

*Department of Astronomy and Astrophysics, University of Toronto,
50 St George Street, M5S 3H4, Toronto, Canada and
Canadian Institute for Theoretical Astrophysics,
60 St George Street, M5S 3H8, Toronto, Canada*

Niayesh Afshordi†

*Department of Physics and Astronomy, University of Waterloo,
200 University Ave W, N2L 3G1, Waterloo, Canada
Waterloo Centre for Astrophysics, University of Waterloo, Waterloo, ON, N2L 3G1, Canada and
Perimeter Institute For Theoretical Physics, 31 Caroline St N, Waterloo, Canada*

Halo Models of large scale structure provide powerful and indispensable tools for phenomenological understanding of the clustering of matter in the Universe. While the halo model builds structures out of the superposition of haloes, defining halo profiles in their outskirts - beyond their virial radii - becomes increasingly ambiguous, as one cannot assign matter to individual haloes in a clear way. In this paper, we tackle this question by using numerical N-body simulations to find a systematic definition of mean halo profile that can be extended to large radii. These profiles must be compensated and are the key ingredients for the computation of cosmological correlation functions in the Amended Halo Model. The latter, introduced in our earlier work [1], provides a more physically accurate phenomenological description of nonlinear structure formation, which respects conservation laws on large scales. Here, we extend this model from the matter auto-power spectrum to the halo-matter cross-power spectra, using N-body simulations. We find that the (dimensionless) compensated halo profile, $r^3 \times \rho(r)/M_{200c}$ has a near-universal maximum in the small range $0.03 - 0.04$ around the virial radius, $r \simeq r_{200c}$, independent of the halo mass. The profiles cross zero into negative values in the halo outskirts, beyond $2-3 \times r_{200c}$, consistent with our previous results. We provide preliminary fitting functions for compensated Navarro-Frenk-White (NFW) profiles, which can be used to compute more physical observables in the Amended Halo Model of large scale structure.

I. INTRODUCTION

Observations and modelling of the large scale structure of the universe is an active area of interest in cosmology. While the interior structure of halos is mostly modelled with the Navarro-Frenk-White (NFW) or Einasto profiles [2, 3], the large scale distribution of dark matter in the outskirts of individual haloes is poorly understood, at least in semi-analytic frameworks. Previous studies have attempted to produce a model using effective field theory (EFT) and perturbation theory [4–7], but nonlinearities in the structure make it difficult to extrapolate beyond $k \geq \text{Mpc}^{-1}$. For smaller scales, the Standard Halo Model is often used as a phenomenological framework, although it

suffers from pathologies that stem from not enforcing of the conservation laws [8]. One proposal to address these pathologies, namely the large-scale shot noise, has been to impose an exclusion radius for haloes [9, 10], but it is hard to see how this would distinguish between the conserved and non-conserved quantities, as the latter are expected to display shot noise on large scales.

In order to address this issue in a systematic manner, we introduced an amended halo model (AHM) in [1] with compensated halo profiles and fitted this to cold dark matter simulations by Takahashi et al. [11] to model nonlinear dark matter density power spectrum on scales of $10^{-2} \text{ Mpc}^{-1} \lesssim k \lesssim 10 \text{ Mpc}^{-1}$. However, this analysis did not consider the profile's potential dependence on halo mass, nor did it

include non-linear biasing in halo-halo correlations (e.g., [12]). Consequently, the present study aims to address these deficiencies. To do this, we adopt simulation data from the Dark-Emu cosmological emulator suite [13] - which uses Planck 2015 cosmology [14] - and develop a novel and systematic method to directly measure mean compensated profiles, from simulated (or emulated) halo-matter and halo-halo correlations. We find that the dimensionless compensated halo profiles all peak around the virial radius, at a near-universal maximum, independent of mass bin, which is quite a striking result. We also find that it is possible to “extrapolate” the NFW profile beyond the virial radius using an extra parameter to fit our compensated halo profile, and provide an approximate functional form (although more parameters are likely necessary if we want a highly accurate numerical fit). While the real physical meaning of this new parameter is yet to be determined, our main goal here is to show that a simple fit for the compensated halo profile can be used to predict the matter-halo cross-correlation, while avoiding the pathologies of standard halo model. Our fit matches NFW in the halo regions $r < r_{\text{virial}}$, but is compensated in the outer regions $r > r_{\text{virial}}$. This paper is then structured as follows: Section II outlines the amended halo model [1] for halo-matter cross correlations, Section III discusses our findings from the results of the simulation data from DarkEmu [13], and Section IV summarizes the results and potential avenues for future research. The exact form of the fitting function we used, and its derivation and implications are outlined in the Appendix.

In this paper, the virial radius r_{virial} is taken to be the radius where density is 200 times the critical density of the universe, or equivalent to r_{200c} . Unless noted otherwise, the mass of a halo is also defined as the total mass contained within this radius.

II. STANDARD VS AMENDED HALO MODELS

In the standard halo model (SHM), the matter overdensity in the universe $\delta(\mathbf{x})$ is described as a superposition of individual halo profiles, that we refer to as w^j :

$$\delta_m(\mathbf{x}) = \bar{\rho}^{-1} \sum_j M_j u_{\text{SHM}}^j(\mathbf{x} - \mathbf{x}_j), \quad (1)$$

in real space, and

$$\delta_{m,\mathbf{k}} = \bar{\rho}^{-1} \sum_j M_j u_{\text{SHM},\mathbf{k}}^j \exp(i\mathbf{k} \cdot \mathbf{x}_j), \quad (2)$$

in Fourier space, where u_{SHM} is the halo profile from the Standard Halo Model (SHM), M_j and \mathbf{x}_j are the mass and position of the j -th halo, respectively, while $\bar{\rho}$ denotes the mean density of the universe. To get a complete understanding of matter distribution, we need to know both how matter is distributed within individual halos, w^j 's, and how these halos are distributed throughout space. Furthermore, conservation laws, such as those of mass and linear momentum, require a fine balance between these two distributions, which are often hard to enforce in the SHM formulation (but see [4]).

In order to address this, we introduced the Amended Halo Model (AHM), where we split the nonlinear overdensities between the linear $\delta_L(\mathbf{x})$ and halo contributions, revising the SHM equations (1) and (2) to be:

$$\delta_m(\mathbf{x}) = \delta_L(\mathbf{x}) + \bar{\rho}^{-1} \sum_j M_j u_{\text{AHM}}^j(\mathbf{x} - \mathbf{x}_j) \quad (3)$$

and

$$\delta_{m,\mathbf{k}} = \delta_{L,\mathbf{k}} + \bar{\rho}^{-1} \sum_j M_j u_{\text{AHM},\mathbf{k}}^j \exp(i\mathbf{k} \cdot \mathbf{x}_j) \quad (4)$$

in real and Fourier spaces, respectively. The nonlinear contribution to the halo profile, w^j , is what we will be calculating from simulations, since the contribution from the linear term is already included in $\delta_L(\mathbf{x})$.

Now, let us consider the overdensity of haloes within a mass-bin b :

$$\delta_{\text{halo},\mathbf{k}}^b = \frac{1}{\bar{n}_{\text{halo}}^b} \sum_j \mathcal{N}_b^j \exp(i\mathbf{k} \cdot \mathbf{x}_j), \quad (5)$$

where $\mathcal{N}_b^j = 1$ if the j -th halo is within the mass-bin b , but vanishes otherwise. Furthermore, \bar{n}_{halo}^b is the number density of haloes within the mass bin.

The cross/auto-power spectrum between the halo and mass distribution can now be defined as:

$$P_{mm}(k) \equiv \frac{\langle \delta_{m,\mathbf{k}} \delta_{m,\mathbf{k}}^* \rangle}{V} \quad (6)$$

$$P_{hh}^{bc}(k) \equiv \frac{\langle \delta_{\text{halo},\mathbf{k}}^b \delta_{\text{halo},\mathbf{k}}^{c*} \rangle}{V} \quad (7)$$

$$P_{hm}^b(k) \equiv \frac{\langle \delta_{\text{halo},\mathbf{k}}^b \delta_{m,\mathbf{k}}^* \rangle}{V}, \quad (8)$$

where V is the volume of the simulation, and b and c stand for different halo mass bins. Now, by multiplying equations (5) and (4), we find the cross-power spectra:

$$P_{hm}^b(k) = b(\bar{M}_b) P_L(k) + \frac{1}{\bar{n}_{\text{halo}}^b \bar{\rho} V} \sum_j M_j \mathcal{N}_b^j u_{\text{AHM},\mathbf{k}}^j \frac{1}{\bar{n}_{\text{halo}}^b \bar{\rho} V} \sum_{j \neq l} M_j \mathcal{N}_b^l u_{\text{AHM},\mathbf{k}}^j \exp[i\mathbf{k} \cdot (\mathbf{x}_j - \mathbf{x}_l)], \quad (9)$$

which we can write in the matrix form:

$$\begin{pmatrix} P_{hm}^1(k) \\ \dots \\ P_{hm}^q(k) \end{pmatrix} = P_L(k) \begin{pmatrix} b(\bar{M}_1) \\ \dots \\ b(\bar{M}_q) \end{pmatrix} + \begin{pmatrix} \bar{M}_1/\bar{\rho} & 0 & \dots & 0 \\ 0 & \bar{M}_2/\bar{\rho} & \dots & 0 \\ \dots & \dots & \dots & \dots \\ 0 & \dots & \dots & \bar{M}_q/\bar{\rho} \end{pmatrix} \begin{pmatrix} u_{\text{AHM}}^1(k) \\ \dots \\ u_{\text{AHM}}^q(k) \end{pmatrix} + \begin{pmatrix} P_{hh}(k|\bar{M}_1, \bar{M}_1) & P_{hh}(k|\bar{M}_1, \bar{M}_2) & \dots & P_{hh}(k|\bar{M}_1, \bar{M}_q) \\ P_{hh}(k|\bar{M}_2, \bar{M}_1) & P_{hh}(k|\bar{M}_2, \bar{M}_2) & \dots & P_{hh}(k|\bar{M}_2, \bar{M}_q) \\ \dots & \dots & \dots & \dots \\ P_{hh}(k|\bar{M}_q, \bar{M}_1) & P_{hh}(k|\bar{M}_q, \bar{M}_2) & \dots & P_{hh}(k|\bar{M}_q, \bar{M}_q) \end{pmatrix} \times \begin{pmatrix} \mu_1 & 0 & \dots & 0 \\ 0 & \mu_2 & \dots & 0 \\ \dots & \dots & \dots & \dots \\ 0 & \dots & \dots & \mu_q \end{pmatrix} \begin{pmatrix} u_{\text{AHM}}^1(k) \\ \dots \\ u_{\text{AHM}}^q(k) \end{pmatrix}. \quad (10)$$

Here, $q \geq 1$ is the number of mass bins used, and we have used the following definitions:

$$\bar{M}_b \equiv \frac{\sum_j \mathcal{N}_b^j M_j}{\bar{n}_{\text{halo}}^b V}, \quad (11)$$

$$\mu_b \equiv \frac{\bar{n}_{\text{halo}}^b \bar{M}_b}{\bar{\rho}}, \quad (12)$$

$$u_{\text{AHM}}^b(k) \equiv \frac{\sum_j \mathcal{N}_b^j M_j u_{\text{AHM},\mathbf{k}}^j}{\bar{n}_{\text{halo}}^b \bar{M}_b V}. \quad (13)$$

Note that, at this level, AHM does not make a prediction for the halo-halo auto-power spectrum, which can be impacted by nonlinear structure formation, and here we rely on N-

body simulations to model it. Furthermore, Equation (9) or (10) can be considered as precise definitions of (mean) halo profiles u_{AHM}^b and linear bias $b(\bar{M}_b)$ (by setting $u_{\text{AHM}}^b(k=0) \rightarrow 0$), and thus make no assumptions about the distribution of matter.

One may then gain an intuition about the nature of the AHM vs SHM on large scales, using the linear bias approximation for halo distribu-

tion, and the mass function $n(M)$:

$$\begin{aligned} \delta_{m,\mathbf{k}} &= \delta_{L,\mathbf{k}} + \sum_j \frac{M^j}{\bar{\rho}} u_{\text{AHM},\mathbf{k}}^j \exp(i\mathbf{k} \cdot \mathbf{x}_j) \\ &\simeq \left[1 + \frac{1}{\bar{\rho}} \int dM M n(M) b(M) u_{\text{AHM}}(k, M) \right] \delta_L(k), \end{aligned} \quad (14)$$

where the fact that $u_{\text{AHM}}^b(k=0) \rightarrow 0$ guarantees the agreement with linear density predictions on large scales. In contrast, for SHM, we have:

$$\delta_{m,\mathbf{k}} \simeq \left[\frac{1}{\bar{\rho}} \int dM M n(M) b(M) u_{\text{SHM}}(k, M) \right] \delta_L(k), \quad (15)$$

where $u_{\text{SHM}}^b(k=0) \rightarrow 1$, and thus an additional condition of $\int dM M n(M) b(M) = \bar{\rho}$ is necessary to recover large scale linear behaviour¹. Even then, as we discussed in [1], the 1-halo term in SHM spoils the linear behavior of the matter power spectrum on large scales, while the revised Equations (1) and (2) are guaranteed to recover it.

III. RESULTS AND DISCUSSION

To find the amended halo profile function $u_{\text{AHM}}(k|M)$ from Eq.(10), we use simulation data from DarkEmu [13] for the auto halo power spectrum P_{hh} , and halo-mass cross-power spectrum P_{hm} . We then invert Eq.(10) to find the halo profile functions, which are plotted in Figure (1), and compared to the best-fit NFW profiles in the corresponding mass bins. Note that all $u_{\text{AHM}}(k|M)$'s go to zero for $k \rightarrow 0$ for compensated haloes, while $u_{\text{NFW}}(k) \rightarrow 1$ by construction as NFW haloes are truncated at r_{virial} . However, even for larger k 's, the profiles don't

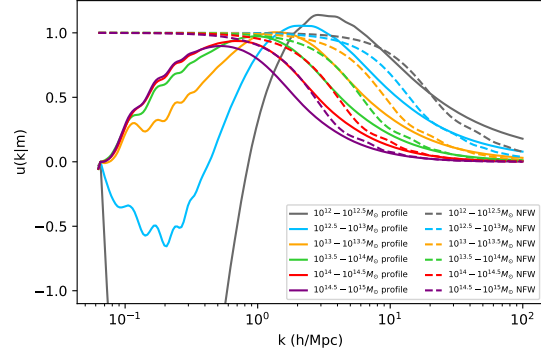


FIG. 1. (a) The $u(k|m)$ function for all mass bins in Fourier space. It can be seen here that the profiles all have a similar peak height, but the peak position k increases as the halo mass decreases. We also see the halo profiles approach the NFW profile at large k 's/small r 's, or inside the halo region, as we should expect (simulation).

exactly match the NFW in Fourier space, with the discrepancy being bigger for smaller mass halos. This is likely due to leakage of structure outside the virial radius into larger k 's, in the Fourier transform.

To investigate this issue, and since we are more used to thinking about profiles in real space, we can Fourier transform the inferred $u_{\text{AHM}}(k|M)$'s to find real-space profiles $u(r) = \rho(r)/M$. Figure (2) shows these real-space profiles, as a function r/r_{virial} . As expected, what we find is that the compensated profile goes negative in the outskirts, just outside the splash-back radii of the haloes [15].

In the inner regions, the dimensionless profile $r^3 \times u(r)$ has a near-universal positive maximum around $r = r_{\text{virial}}$ (with values ranging from 0.034 to 0.039, for smallest to largest masses). The profile is also mostly independent of the minimum mass bin of the halo with a key exception - for results to be reasonable, the smallest mass bin should be $\geq 10^{12} M_{\odot}$ - which is set by the minimum mass of haloes resolved in DarkEmu simulations.

Figure (3) shows the enclosed mass (in units of virial mass), that results from integrating

¹ While this condition follows from the assumption that all mass is in haloes, given that $b(M)$ and $n(M)$ are measured from simulations only in a finite mass range, satisfying $\int dM M n(M) b(M) = \bar{\rho}$ requires an additional constraint on extrapolating functions

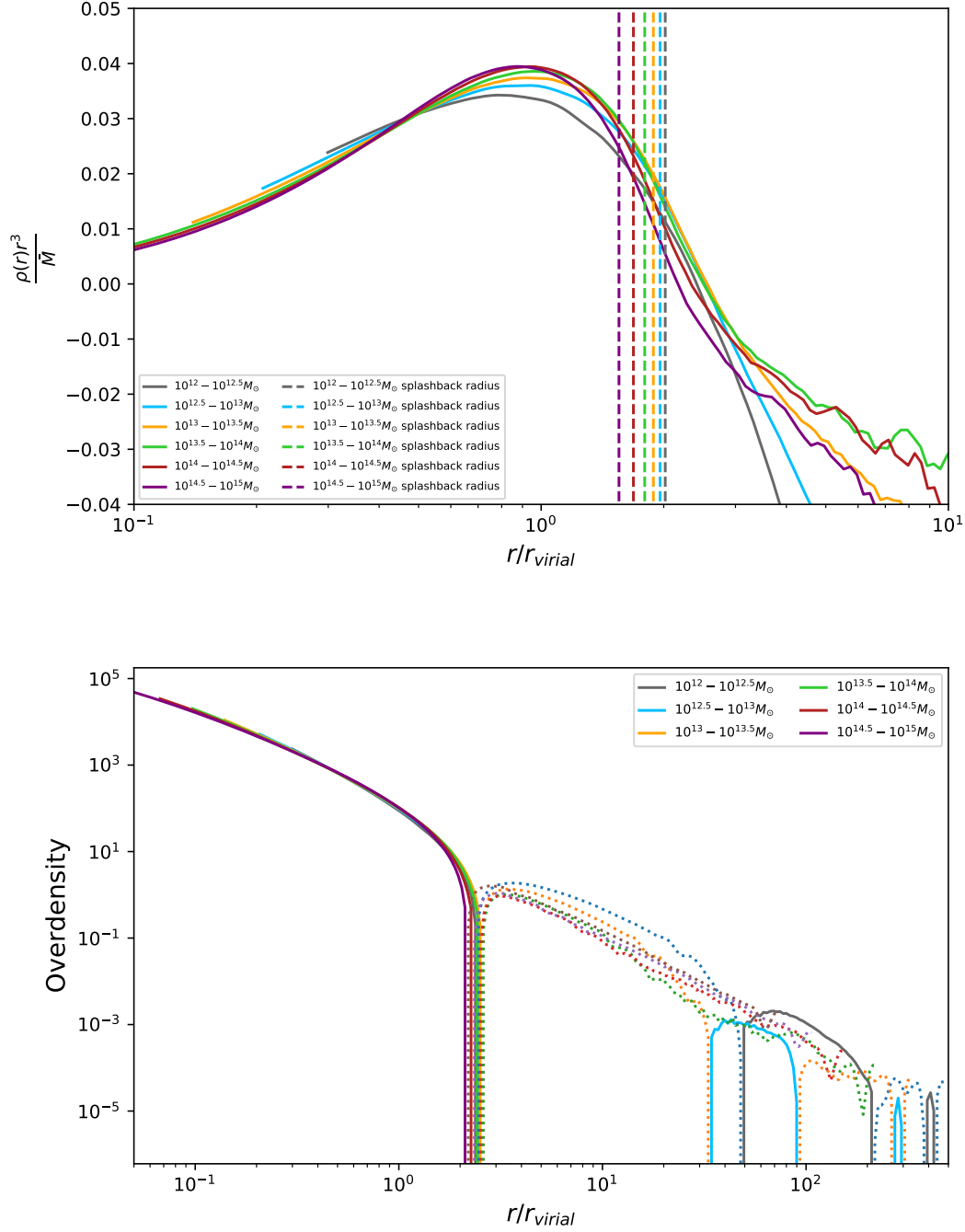


FIG. 2. This figure shows the halo profile $u(r)$ in real space. In panel (a)(top) the profile is multiplied by r^3 , and plotted as a function of $r/r_{virial} = r/(cr_{scale})$ up to 10 times the virial radius. This shows that the dimensionless profile peaks around r_{virial} and has near-universal values for all mass bins. The zero crossing happens at distances 20% – 30% outside the splashback radii of the haloes, that are shown for comparison [15]. In panel (b) (bottom), the halo overdensities $\rho(r)/\bar{\rho}$ for each mass bin in real space are shown for our entire radial range, although they are not reliable at very large distances. The dotted parts show negative overdensity.

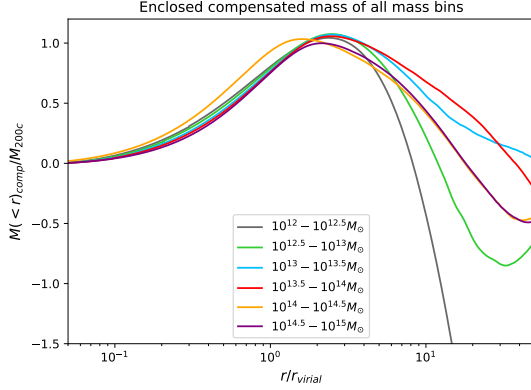


FIG. 3. The integrated enclosed mass found in real space using the compensated halo profile. Similar to the halo profiles, the peak height of the enclosed masses for different mass bins are also almost the same, independent of mass bin size.

Mass bin	β	α	r_{zc}	$\frac{r_{zc}}{r_{vir}}$	r_{peak}	$\frac{r_{peak}}{r_{vir}}$
$10^{12}-12.5 M_{\odot}$	1.7×10^{-7}	0.78	0.65	3.1	0.21	0.98
$10^{12.5}-13 M_{\odot}$	4.6×10^{-7}	0.80	0.87	2.9	0.30	0.98
$10^{13}-13.5 M_{\odot}$	1.2×10^{-6}	0.77	1.2	2.8	0.45	1.0
$10^{13.5}-14 M_{\odot}$	2.2×10^{-6}	0.75	1.8	2.8	0.65	1.0
$10^{14}-14.5 M_{\odot}$	6.7×10^{-6}	0.76	2.3	2.5	0.91	0.97
$10^{14.5}-15 M_{\odot}$	1.5×10^{-5}	0.77	3.2	2.3	1.3	0.94

TABLE I. Best fit parameters for Eq. (A2) shown by α and β . We also report the best-fit zero-crossing radius r_{zc} , the ratio of the zero-crossing radius and the virial radius r_{zc}/r_{vir} , the peak radius r_{peak} (where $u(r)r^3$ is at a maximum), as well as the ratio of the peak radius to the virial radius.

Figure (2)². The radii of the peaks of these mass profiles would thus coincide with zero crossings of the density. We further notice that the maximum compensated masses (masses of compensated halos) are nearly the same as uncompensated virial mass, although the latter is defined at a smaller radius.

² We use the NFW profile to integrate mass within radii below the spatial resolution of the DarkEmu

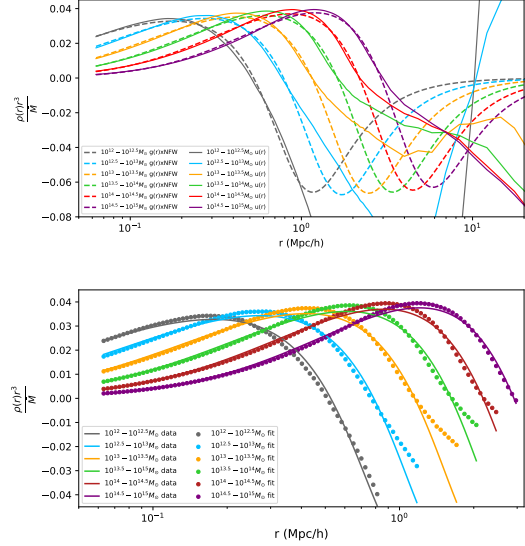


FIG. 4. (a)(Top) The $u(r)$ function times r^3 in real space compared to the NFW profile. It can be seen that at small r 's, the two start to approach each other, as we would expect, since NFW describes halo density at small radii inside the halo (this likely deviates near the halo centre due to baryonic effects, but we don't go to that scale here). (b) (Bottom) The $u(r)$ ($u(k|m)$ function Fourier transformed into real space) fitted to a function with two free parameters (see Table 1). The fit works up to around 1-4Mpc/h, after which the Fourier transform noise takes over.

In Figure 4, we fit our measured halo profiles in real space to a function of the form

$$M \times u_{\text{AHM}}(r|M) = g(r) \times \rho_{\text{NFW}}(r), \quad (16)$$

where ρ_{NFW} is the best-fit NFW profile for the corresponding mass bin, and $g(r)$ is a simple fitting function (with two free parameter α and β) that approaches α at small r , but goes negative at $r > r_{zc}$, and is constructed such that $g \times \rho_{\text{NFW}}$ is compensated (see A for the full form of $g(r)$).

Table I shows our numerical best fits for α and β for each mass bin. We also see that, as we noted above, the peak of $r^3 \times u(r|M)$ is always within a few percent of the virial radius, while the zero crossing happens at r_{zc} , between 2-3 times the virial radius (or 1.2-1.3 times the

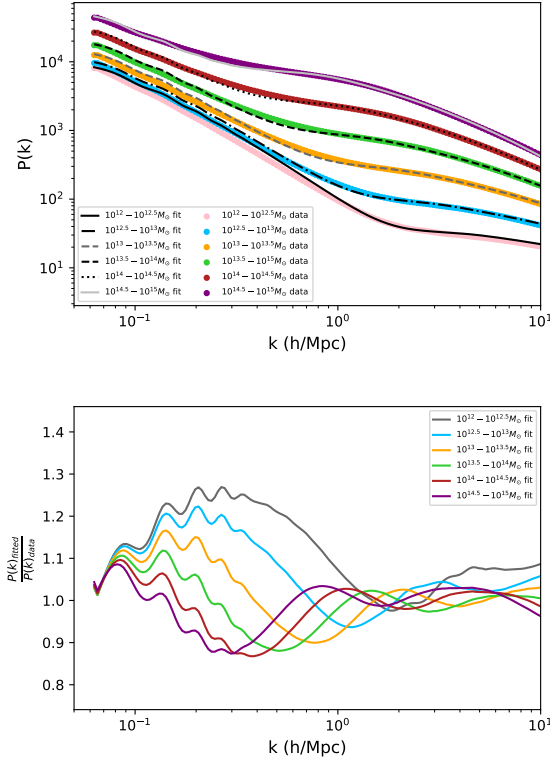


FIG. 5. (a) (top) Comparison of matter-halo cross-power spectra, between DarkEmu (dots) and our fitted compensated profiles (Equation 16). (b) (bottom) The ratio of our analytic fit to DarkEmu cross-power spectra for each mass bin. The fit works better for larger mass bins, where the DarkEmu simulation data is more robust. Moreover, note that the fit in Equation (16) is only done in real space and radii $r < 3 h^{-1}\text{Mpc}$, which is why the behavior at smaller k 's is not well-modelled by the fit. Furthermore, $k > \text{Mpc}^{-1}$ are not well-resolved in DarkEmu.

splashback radius, see Figure 2).

Using this fitted halo profile to account for compensation, we re-calculated the power spectrum to see how well it matched the data from DarkEmu. The results are shown in the top and bottom plots of Figure 4, which shows that our theoretical fit is capable of matching the simulation data within the range where the halo profile is not noise dominated (both inside and outside the halo regions).

From the Figures 4 (a) and (b), it can be seen that it is possible to fit the cross halo-matter power spectrum using a compensated halo profile term as well. While, so far our fitted β parameters do not have a straightforward physical interpretation (α is only a simple normalization), our exercise shows that both the matter auto spectrum, as well as the matter-halo cross power spectra, can be modelled with compensated halo profiles. Figure 5 compares the resulting cross-power spectra from Equation (16) with DarkEmu, showing reasonable agreement at small scales (used in the fit), but modest 20 – 30% disagreement for larger scales. For practical applications, the accuracy of the fit can be improved if more parameters are added, but that is beyond the scope of this study.

IV. CONCLUSION AND FUTURE PROSPECTS

In this paper, we built upon our previous study [1], to show that compensation – introduced as an important amendment of the halo model to respect physical conservation laws – can be applied to model the auto-matter power spectrum, as well as the halo-matter cross-power spectra. Compensated halo profiles still match NFW in the inner halo regions, but now also take into account underdense regions (or voids) in the outskirts of cosmological haloes. The new compensated (dimensionless) profiles show a near-universal behavior out to the splashback radius, independent of the halo mass. Notable the dimensionless profile peaks at the virial radius, and the maximum compensated mass coincides with the (uncompensated) virial mass of the haloes. This new profile can also be fitted numerically by introducing two free parameters, which we report in Table I. The physical interpretation the fitting parameters, are currently beyond the scope of this paper, and we leave them for future work. Furthermore, more precise fits (outside $r \gtrsim h^{-1}\text{Mpc}$ can be obtained by using more parameters in the fitting function. This will be an important step to compare the predictions of

the amended halo profile for weak lensing and kinetic Sunyaev-Zel'dovich (kSZ) observations, where mass and momentum conservation may play an important role in constraining physical possibilities on intermediate and large scales.

Other factors not taken into account here are sub-structure of halos, and halo assembly bias [16] - for the latter, we did try different bias models ([17], [12]), but it did not yield any significant changes in the results. Effects that assembly bias, halo sub-structure, or filaments may further have on the compensated halo profiles are interesting future prospects to explore. In particular, the extent to which AHM can be used (or adapted) to model the matter/halo bispectra (or 3-point correlation function) is another interesting direction, as it may probe the covariance of compensated profiles at large distances; an important step for kSZ studies will be the determination of compensated momentum profiles (due to gas infall in halo outskirts) in the hydrodynamical simulations. Furthermore, the mass clustering in haloes will affect the rotation curves of the galaxies residing inside these haloes [18], which can provide evidence for different cosmological models, such as Λ CDM vs. MOND [18]. All these effects are interesting future paths of exploration for dark matter halo profiles.

ACKNOWLEDGMENTS

We would like to thank Jenny Wagner, Vincent Desjacques, Alexander Mead, Fabian Schmidt, and Dejan Stojkovic for helpful discussions, suggestions, and comments.

We would also like to thank Ryuichi Takahashi, Masanori Sato, Takahiro Nishimichi, Atsushi Taruya, and Masamune Oguri for letting us use their large scale simulation data for the matter auto-power spectra, as well as the Dark-Emu team for their halo-matter cross-power spectra simulation data [13]. For calculating linear and numerical nonlinear power spectra for comparison with our model, we used the CAMB package in Python [11, 19, 20].

AC was funded by the Department of Astronomy and Astrophysics at University of Toronto and the Canadian Institute for Theoretical Astrophysics (CITA). NA is funded by the University of Waterloo, the National Science and Engineering Research Council of Canada (NSERC) and the Perimeter Institute for Theoretical Physics. Research at Perimeter Institute is supported by the Government of Canada through Industry Canada and by the Province of Ontario through the Ministry of Economic Development & Innovation.

Appendix A: Explicit profiles

The NFW function in Fourier space is given by:

$$u_{\text{NFW}}(k|M) = \frac{4\pi\rho_s r_s^3}{M} \left\{ \sin(kr_s)(\text{Si}[(1+c)kr_s] - \text{Si}(kr_s)) + \cos(kr_s)(\text{Ci}[(1+c)kr_s] - \text{Ci}(kr_s)) - \frac{\sin(ckr_s)}{(1+c)kr_s} \right\}, \quad (\text{A1})$$

and this is the equation that our fitting function tends to in the limit $r \ll r_{\text{virial}}$.

The fitting function $g(r)$ in Eq. 16 is of the form

$$g(r) = \alpha \left(1 - \frac{\sqrt{\beta}(-4(1+\beta)+\beta^{1/4}(2\sqrt{2}-3\beta^{1/4}+4\sqrt{2\beta}-2\sqrt{2\beta+\beta^{5/4}})\pi+(-1+3\beta)\ln(\beta))(r/r_{scale})^2}{\pi(1-2\sqrt{2}\beta^{1/4}+4\sqrt{2}\beta^{3/4}-3\beta+2\sqrt{2}\beta^{5/4})+\sqrt{\beta}(-4(1+\beta)+\ln(\beta)(\beta-3))} \right) \frac{(r/r_{scale})^2}{1 + \beta \left(\frac{r}{r_{scale}}\right)^4}, \quad (\text{A2})$$

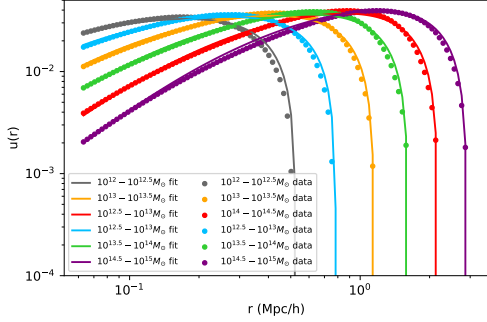


FIG. 6. A comparison of the simulation halo profile (scatter points) and our compensated profile $u(r)$ in Fourier space, zoomed in at smaller r 's.

where α and β are parameters fitted by least square fitting, listed in Table I. This function is designed to be of the form

$$g(r) \propto \frac{1 - s(\beta)r^2}{1 + \beta r^4}, \quad (\text{A3})$$

where $s(\beta)$ is found by integrating $g(r) \times \rho_{\text{NFW}}$ from 0 to infinity and setting the integral to 0. As a result, the final halo profile is compensated.

* ay7chen@uwaterloo.ca

† nafshordi@pitp.ca

- [1] A. Y. Chen and N. Afshordi, Amending the halo model to satisfy cosmological conservation laws, *Phys. Rev. D* **101**, 103522 (2020), arXiv:1912.04872 [astro-ph.CO].
- [2] J. F. Navarro, C. S. Frenk, and S. D. M. White, The Structure of cold dark matter halos, *Astrophys. J.* **462**, 563 (1996), arXiv:astro-ph/9508025 [astro-ph].
- [3] A. D. Ludlow and R. E. Angulo, Einasto Profiles and the Dark Matter Power Spectrum, *Mon. Not. Roy. Astron. Soc.* **465**, L84 (2017), arXiv:1610.04620 [astro-ph.CO].
- [4] F. Schmidt, Towards a self-consistent halo model for the nonlinear large-scale structure, *Phys. Rev.* **D93**, 063512 (2016), arXiv:1511.02231 [astro-ph.CO].
- [5] U. Seljak and Z. Vlah, Halo Zel'dovich model and perturbation theory: Dark matter power spectrum and correlation function, *Phys. Rev.* **D91**, 123516 (2015), arXiv:1501.07512 [astro-ph.CO].
- [6] N. Hand, U. Seljak, F. Beutler, and Z. Vlah, Extending the modeling of the anisotropic galaxy power spectrum to $k = 0.4 \text{ hMpc}^{-1}$, *JCAP* **1710** (10), 009, arXiv:1706.02362 [astro-ph.CO].
- [7] O. H. E. Philcox, D. N. Spergel, and F. Villaescusa-Navarro, Effective halo model: Creating a physical and accurate model of the matter power spectrum and cluster counts, *Phys. Rev. D* **101**, 123520 (2020), arXiv:2004.09515 [astro-ph.CO].
- [8] A. Cooray and R. K. Sheth, Halo Models of Large Scale Structure, *Phys. Rept.* **372**, 1 (2002), arXiv:astro-ph/0206508 [astro-ph].
- [9] D. Ginzburg, V. Desjacques, and K. C. Chan, Shot noise and biased tracers: A new look at the halo model, *Phys. Rev. D* **96**, 083528 (2017), arXiv:1706.08738 [astro-ph.CO].
- [10] O. Umeh, R. Maartens, H. Padmanabhan, and S. Camera, The effect of finite halo size on the clustering of neutral hydrogen, *JCAP* **06**, 027, arXiv:2102.06116 [astro-ph.CO].
- [11] R. Takahashi, M. Sato, T. Nishimichi, A. Taruya, and M. Oguri, Revising the Halofit Model for the Nonlinear Matter Power Spectrum, *Astrophys. J.* **761**, 152 (2012), arXiv:1208.2701 [astro-ph.CO].

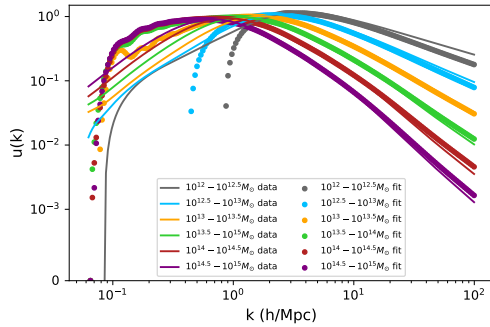


FIG. 7. A comparison of the simulation halo profile (scatter points) and our compensated profile $u(k|m)$ in Fourier space, zoomed in at smaller k 's. It can be seen here that even though the compensated profile matches the data fairly well in real space at large r 's, the same isn't true for small k 's, so the relation between the two isn't exactly proportional due to k -mode mixing.

- [12] A. J. Mead and L. Verde, Including beyond-linear halo bias in halo models, *Mon. Not. Roy. Astron. Soc.* **503**, 3095 (2021), arXiv:2011.08858 [astro-ph.CO].
- [13] T. Nishimichi *et al.*, Dark Quest. I. Fast and Accurate Emulation of Halo Clustering Statistics and Its Application to Galaxy Clustering, *Astrophys. J.* **884**, 29 (2019), arXiv:1811.09504 [astro-ph.CO].

- [14] P. A. R. Ade *et al.* (Planck), Planck 2015 results. XV. Gravitational lensing, *Astron. Astrophys.* **594**, A15 (2016), arXiv:1502.01591 [astro-ph.CO].
- [15] S. More, B. Diemer, and A. Kravtsov, The splashback radius as a physical halo boundary and the growth of halo mass, *Astrophys. J.* **810**, 36 (2015), arXiv:1504.05591 [astro-ph.CO].
- [16] N. Dalal, M. White, J. Bond, and A. Shirokov, Halo Assembly Bias in Hierarchical Structure Formation, *Astrophys. J.* **687**, 12 (2008), arXiv:0803.3453 [astro-ph].
- [17] J. L. Tinker, A. V. Kravtsov, A. Klypin, K. Abazajian, M. S. Warren, G. Yepes, S. Gottlober, and D. E. Holz, Toward a halo mass function for precision cosmology: The Limits of universality, *Astrophys. J.* **688**, 709 (2008), arXiv:0803.2706 [astro-ph].
- [18] D.-C. Dai, G. Starkman, and D. Stojkovic, Milky Way and M31 rotation curves: Λ CDM versus MOND, *Phys. Rev. D* **105**, 104067 (2022), arXiv:2201.06034 [astro-ph.GA].
- [19] A. Lewis, A. Challinor, and A. Lasenby, Efficient computation of CMB anisotropies in closed FRW models, *Astrophys. J.* **538**, 473 (2000), arXiv:astro-ph/9911177 [astro-ph].
- [20] J. A. Peacock and R. E. Smith, Halo occupation numbers and galaxy bias, *Mon. Not. Roy. Astron. Soc.* **318**, 1144 (2000), arXiv:astro-ph/0005010 [astro-ph].